Ship detection and characterization using polarimetric SAR

R. Touzi and F. Charbonneau and R.K. Hawkins and P.W. Vachon

Canada Centre for Remote Sensing

Natural Resources Canada

588 Booth Street, Ottawa

Ontario, Canada K1A OY7

phone: 613-947-1247, fax: 613-947-1383, email: ridha-touzi@ccrs.nrcan.gc.ca

Abstract

Polarimetric information is investigated for ship detection and characterization at operational satellite SAR incidence angles (20° to 60°). It is shown that among the conventional single channel polarizations (HH, VV, or HV), HV provides the best ship-sea contrast at incidence angles smaller than 50°. Furthermore, HH polarization permits the best ship-sea contrast at near grazing incidence angles. The polarization anisotropy is often used for optimal information extraction from polarimetric SAR data. It is shown that fully polarimetric information permits a significant improvement in the ship-sea contrast for relatively calm wind conditions, in comparison with conventional (i.e., scalar) single channel polarizations (i.e., HH, VV, or HV). For rougher sea conditions, the effectiveness of polarimetric tools may be significantly degraded. Ship characterization is also investigated using the symmetric scattering characterization method (SSCM). Identification of ship targets with significant symmetric scattering can provide a useful ship pitch angle estimate, under certain conditions.

RESUMÉ

L'apport de l'information polarimétrique à la détection et la caractérisation des bateaux est étudiée. Parmi les polarisations conventionnelles HH, VV, et HV, la polarisation HV permet le meilleur contraste bateau-mer aux angles d'incidence plus petits que 50°. HH donne les meilleurs résultats aux incidences rasantes. L'anisotropie de polarisation a été utilisée pour l'extraction optimale de l'information polarimétrique. La polarimétrie permet une grande amélioration du contraste bateau-mer dans des conditions de mer et vents relativement calmes. L'efficacité de la polarimétrie est réduite quand la mer est agitée. La méthode SSCM a été testée pour la caractérisation de bateaux. Elle a même permis une mesure de l'angle de tangage de bateaux dans certaines conditions.

under contract with TGIS Consultant
currently seconded to Defence R&D Canada - Ottawa

LIST OF FIGURES AND TABLES

I. Introduction

Ship detection and identification has many potential applications within the commercial, fishery, vessel traffic service, and military sectors. The importance of the transmit-receive antenna polarizations on ship detectability is now well understood. Better ship-sea contrast is obtained with HH polarization, whereas VV polarization provides more information on the sea surface conditions [29], [4], [17]. Future satellite SARs will offer various polarization channels, and as such, will be able to provide additional information that will permit better characterization of the illuminated targets. For example, the ENVISAT ASAR [31] allows simultaneous measurement of two polarization channels (chosen from among the four linear polarizations HH, VV, HV, and VH) in the alternating polarization mode. Furthermore, RADARSAT-2 [15] and ALOS-PALSAR [12] will be fully polarimetric SARs. With these upcoming polarimetric missions, it is important to assess the ship-sea contrast improvement that can be obtained by using the additional polarization information. On the other hand, it is well known that fully polarimetric data has a strong potential for characterization of target backscattering [3], [23], [22]. Such information might be helpful for ship identification and for ship orientation (i.e., pitch and roll) estimation.

In this study, ship detection and characterization are investigated using fully polarimetric SAR data. Data acquisition and calibration are described in Section 2. In Section 3, ship-sea contrast is analyzed for conventional single channel polarizations (HH, VV, or HV), at operational satellite SAR incidence angles (20° to 60°). The polarization anisotropy, introduced in [21], is also investigated. Ship-sea contrast improvement is then discussed as a function of the SAR illumination angle and wind conditions. In Section 4, ship identification and characterization are investigated with reference to available ground truth data collected during SAR data acquisition. The symmetric scattering characterization method (SSCM), which was introduced in [22], is used for high-resolution characterization of ship scattering. Finally, the potential of the SSCM method for ship identification and pitch angle estimation, is discussed.

II. Polarimetric SAR data collection and calibration

A. Convair-580 Data Acquisition

To cover operational satellite SAR incidence angles (20° to 60°), several data sets were collected with the Environment Canada Convair-580 SAR [14] in two separate experimental trials: Halifax'98 [9] and Crusade'00 [10]. The Halifax'98 trial data were collected off the coast of Nova Scotia and include an area with several ships that were imaged under calm wind conditions within an incidence angle range of 40° to 70°. Unfortunately, the ships were not ground-truthed during SAR data acquisition, so this data set will only be analyzed in terms of ship detectability.

The Crusade'00 trial data were collected off Cape Race, Newfoundland in March, 2000 [10] at lower incidence angles (20° to 55°). During the Crusade'00 trial, the ships were almost stationary and were well

ground-truthed [10], [30], [7]. In this study, the polarization information will be investigated with reference to the ground truth data for two ships; the 18 m long Arctic Pride (AP) (Figure 1) and the 35 m long Anne S Pierce (ASP) (Figure 2). ASP was imaged on March 28 off Cape Race at 22° and 35° incidence angles during winds of 7 kts and waves of 4 m significant height. AP was imaged at a 44° incidence angle on March 28 and again on March 30, the latter during winds of 20 kts and waves of 5 to 6 m significant height. The March 28 case is hereafter referred to as calmer conditions, while the March 30 case is referred to as rougher conditions.

B. Polarimetric data calibration

In order to exploit the fully polarimetric capability of the Convair-580 SAR, pure HH, VV, HV, and VH data must be retrieved from the distorted measurements. In contrast to most existing polarimetric SARs, the Convair-580 SAR uses two receive configurations for each of the H and V transmit polarizations [14]. A general polarimetric model that includes systems with a receive configuration that is independent of the transmit polarization (one configuration), as well as systems with two distinct receive configurations, was introduced in [24]. This model was used to develop a calibration method for the early X-band polarimetric SAR that was developed at CCRS [24].

A simplified method was adapted for the C-band SAR system that is equipped with polarization switches characterized by high isolation (better than 50 dB) [25], [14], [8], [20], [6]. As the H and V antennas are well isolated (better than 35 dB) and their phase centers are co-located, the system can be calibrated using a corner reflector and a recirculating 45°-45° polarimetric active radar calibrator (PARC) placed at the same incidence angle as the corner reflectors. Since the H and V antenna phase centers are co-located, and using knowledge of the H and V antenna gain patterns (with an accuracy of ± 0.5 dB within ±20° of the boresight angle [5]), allows extension of the calibration to over ±20° from the boresight angle [25], [14], [8], [20]. This leads to accuracy within 1 to 2 dB in radiometry and within 5° in phase [20], [8].

It must be noted that, for an antenna depression angle of 39°, the ASP imaged at 22° incidence angle is outside of the required antenna beam angle interval noted above. However, data collected at this incidence angle were calibrated by using reference point targets that were deployed at this particular incidence angle.

III. Ship-sea contrast optimization using polarization information

A. Potential of conventional linear polarizations (HH, VV, and HV) for ship detection

Figure 3 presents the ship-sea contrast calculated for the three linear polarizations for the various ships imaged within the incidence angle range of 20° to 70°. Figure 3 includes the results obtained from the Halifax'98 trail, in which ships were imaged under calm wind conditions within the incidence angle range of 47° to 70° (Figure 4) as well as those obtained from the ASP at 22° and 35° from March 28, and AP at

44° on March 28 and March 30.

From Figure 3, it is apparent that HV gives the highest ship-sea contrast at low incidence angles in comparison to HH and VV polarizations. However, at near grazing incidence angles (larger than 55°), HH, which minimizes the sea return, gives the best contrast. As expected, VV, which is more suitable for sea surface characterization [29], gives the lowest ship-sea contrast over the range of incidence angles considered.

B. Polarization anisotropy for ship detection

Touzi et al. [23] have shown that the extrema of the degree of polarization of the scattered wave permits characterization of target scattering mechanism complexity. Bicout and Brosseau introduced a measure of the wave entropy S which is analytically related to the degree of polarization p by [1]:

$$S(p) = -ln[\,0.5 \cdot (1+p)^{(1+p)/2)} \cdot (1-p)^{(1+p)/2)}\,] \tag{1}$$

$S(p)$ provides a measure of the entropy of the scattered wave. It is directly related to the degree of polarization p that characterizes the purity of the scattered wave. $S(p)$ is a bijective strictly decreasing function of p, which takes values S lying within a finite interval; $S(p = 1) < S < S(p = 0)$. The normalized wave entropy $S_n(p) = S(p)/S(0)$ takes values between 0 and 1. The entropy S_n is zero when the scattered wave is completely polarized, and S_n reaches unity for a completely unpolarized wave ($p = 0$). Variations of the scattered wave purity p with the transmit wave polarization generates variations of the wave entropy. The dynamic range of the entropy ΔS_n, which is directly related to the dynamic range of the degree of polarization Δp, should provide a measure of the complexity of target scattering mechanisms, as shown in [23]. This leads to the following expression for the polarization anisotropy introduced in [21]:

$$\Delta S_n = S_n(p_{min}) - S_n(p_{max}) \tag{2}$$

where the extrema of the degree of polarization, p_{min} and p_{max}, are derived using the analytical method introduced in [23]. The polarization anisotropy, ΔS_n, was introduced to characterize target nonstationarity; the higher ΔS_n, the larger the signal variations with transmit-receive polarization. ΔS_n, which was shown to be an effective tool for ship-sea contrast improvement, is investigated in the following.

Figure 5 shows ΔS_n for the Halifax'98 trail. At low incidence angles, the ocean provides a very homogeneous and pure scattering mechanism, as demonstrated in [23] using the NASA/JPL San Francisco AIRSAR image. This result is confirmed using the Convair-580 SAR data; the ocean generally has a lower ΔS_n in comparison with that of a ship for incidence angles up to 60°. Ships that can hardly be seen in the HH polarization image of Figure 4 are well discriminated in Figure 5. ΔS_n permits a significant improvement in ship-sea contrast, as quantified in Figure 3. At incidence angles higher than 60°, the ocean

backscattering mechanism becomes more heterogeneous and the polarization anisotropy ΔS_n can no longer be used to discriminate a ship from the sea surface clutter.

The same results are confirmed at $22°$ and $35°$ incidence angles with Crusade'00 data collected under calmer conditions. The ΔS_n performance is also significantly degraded for rougher conditions, as seen in Figure 3 for the AP at $44°$ incidence angle. This small ship has a slightly better contrast with ΔS_n in comparison with that of HV polarization.

IV. Ship characterization

A. Optimum polarimetric information extraction

The polarization anisotropy used above, which is generally applied with a large window (9 pixels by 9 pixels) for accurate estimation of the scattered wave characteristics, is not suitable for applications that require high-resolution data, such as ship identification. Partially coherent target decomposition methods (PCTD), such as the Huynen and Cloude methods [11], [3], which extract the polarization information from multi-look Mueller, covariance, or coherency matrices are also not suitable. Ship identification requires the use of coherent target decomposition methods (CTD), such as the Huynen, Krogager, and Cameron methods [11], [13], [2], which extract the polarization information from the high-resolution, 1-look scattering matrix.

Cameron's CTD was reconsidered in [22]. This method, which was inspired by the work of Huynen [11], associates importance to a class of targets termed symmetric. A symmetric target is defined by [11] as a target having an axis of symmetry in the plane orthogonal to the radar line of sight direction (LOS). Symmetric targets have a scattering matrix, which can be diagonalized by a rigid rotation about the LOS in a basis of linear eigen polarizations.

Cameron developed an algorithm that maximizes the symmetrical component of coherent scattering [2], which is then expressed as the sum of independent elements in order to associate a physical mechanism with each component. For operational use of his CTD, Cameron introduced a classification method [2] that has been widely used for characterization and identification of point targets such as ships [18], [30] and small airplanes [16]. Unfortunately, it was shown in [22] that Cameron's classification yields mis-leading results because of the significant radiometric dispersion that is tolerated (up to ± 8 dB), and the absence of criteria that avoids the application of the CTD decomposition method in areas of non-coherent scattering. A new method, referred to as the symmetric scattering characterization method (SSCM), was introduced in [22] to better exploit the information provided by the largest target symmetric scattering component. The SSCM, which expresses the symmetric scattering in terms of the target's Poincaré sphere parameters, permits a high resolution characterization of target symmetric scattering under coherent conditions.

B. The SSCM method for characterization of symmetric scattering

C. Maximization of symmetric scattering

Under target and SAR system reciprocity assumptions, the target scattering matrix is expressed in terms of the Pauli matrices as [2]:

$$[S] = \alpha[S_a] + \beta[S_b] + \gamma[S_c] \tag{3}$$

where

$$[S_a] = \frac{1}{\sqrt{2}} \begin{bmatrix} 1 & 0 \\ 0 & 1 \end{bmatrix} \tag{4}$$

$$[S_b] = \frac{1}{\sqrt{2}} \begin{bmatrix} 1 & 0 \\ 0 & -1 \end{bmatrix} \tag{5}$$

$$[S_c] = \frac{1}{\sqrt{2}} \begin{bmatrix} 0 & 1 \\ 1 & 0 \end{bmatrix} \tag{6}$$

Scattering is symmetric if there exists an angle of rotation ψ_a that cancels the projection of $[S]$ of equation (3) on the non-symmetric Pauli direction $\vec{S}_c$, where $\vec{S}_c$ is the vectorial form of the Pauli matrix $[S_c]$. This leads to the following expression for the symmetric part, $\vec{S}_{sym}$, as a function of the angle $\theta = -2\psi_a$ [2]:

$$\vec{S}_{sym} = \alpha\vec{S}_a + \epsilon \cdot [\cos\theta \cdot \vec{S}_b + \sin\theta \cdot \vec{S}_c] \tag{7}$$

The symmetric component $\vec{S}_{sym}$ of the total scattering $\vec{S}$ (the vector form of $[S]$), reaches its maximum for the angle θ that satisfies the following relationship, for $\beta \neq \gamma$ [2]:

$$\tan(2\theta) = \frac{\beta\gamma^* + \beta^*\gamma}{|\beta|^2 - |\gamma|^2} \tag{8}$$

After diagonalization, the largest symmetric component $\vec{S}_{sym}^{max}$ can be expressed in the trihedral-dihedral basis, $(\vec{S}_a, \vec{S}_b)$, as:

$$\vec{S}_{sym}^{max} = \alpha\vec{S}_a + \epsilon\vec{S}_b \tag{9}$$

where ϵ is given by:

$$\epsilon = (\beta\cos\theta + \gamma\sin\theta) \tag{10}$$

D. Poincaré sphere for representation of symmetric scattering

The maximized symmetric component $\vec{S}_{sym}^{max}$ is characterized by the two complex entities α and ϵ of equation (9). After normalization by the total intensity $(|\alpha|^2 + |\epsilon|^2)$, each diagonalized symmetric scattering vector $\vec{\Lambda}$ was expressed as a function of the Target Poincaré Sphere angles ψ_c and χ_c, as:

$$\vec{\Lambda} = \begin{bmatrix} 1 & \cos(2\chi_c)\cos(2\psi_c) & \cos(2\chi_c)\sin(2\psi_c) & \sin(2\chi_c) \end{bmatrix} \tag{11}$$

where ψ_c and χ_c can be derived as a function of the target parameters α and ϵ of equation (9). Each symmetric scatterer can then be represented as a point of latitude $2\psi_c$ and longitude $2\chi_c$ on the target Poincaré sphere shown in Figure 6.

To remove the rotation phase ambiguity, only half of the sphere is used with ψ_c varying within the interval $[0, \pi/2]$. If ψ_c is lying in the interval $]\pi/2, \pi]$, symmetric scattering sphere coordinates (ψ_c, χ_c) are replaced with $(\pi - \psi_c, -\chi_c)$, and the rotation angle ψ_a of equation (7) is replaced with $\psi_a \pm \pi/2$.

Only a coherent symmetric scatterer can be represented as a point on the surface of the Poincaré sphere. A partially coherent symmetric scatterer is represented as a point inside the sphere at a distance from the sphere center determined by the degree of coherence of the scatterer components α and ϵ on the basis $(\vec{S}_a, \vec{S}_b)$ given by [22]:

$$p_{sym} = \frac{\sqrt{(<|\alpha|^2 - |\epsilon|^2>)^2 + 4.|<\alpha.\epsilon^*>|^2}}{<|\alpha|^2 + |\epsilon|^2>} \tag{12}$$

The parameter p_{sym}, called the degree of symmetric scattering coherence, will be used in the following to limit the application of the SSCM within coherent areas.

E. SSCM scheme

The SSCM includes the following steps [22]:

1. Calculation of the parameters α and ϵ of the maximum symmetric component, using Cameron's CTD [2];

2. Classification of distributed target scattering into coherent and non coherent classes using p_{sym} information;

3. Classification of point target scattering into coherent and non-coherent classes using the Rician threshold [22];

4. Computation and analysis of the S_{max} Poincaré sphere parameters within the coherent class.

In the following, the SSCM is applied for ship characterization using Crusade'00 trail data collected over the AP and the ASP.

F. Ship characterization using the SSCM

F.1 The Arctic Pride (AP)

During the Crusade'00 trail, AP was imaged at $44°$ incidence angle with an orientation of $20°$ from azimuth, on March 28 and 30. The mast near the middle of the ship and the metallic feature near the stern of the ship, referred to as MID and DB in Figure 1, are potential targets of symmetric scattering. Table 1 presents their coordinates (ψ_c, χ_c) on the target Poincaré sphere. They correspond to a signal-to-clutter ratio of about 20 dB, which results in an uncertainty in phase of $\pm 5°$, according to the Rice

distribution [22]. The (MID) mast coordinates appear stable, within the expected $5°$ phase accuracy, during the two acquisitions. The rougher conditions of March 30 did not modify the scattering type of the mast, which is close to pure dipole scattering of coordinates ($\psi_c = 45°$, $\chi_c = 0°$) in the target Poincaré sphere of Figure 6. Since the ship is almost oriented parallel to the azimuth direction (with an orientation angle of about $20°$), the rotation angle ψ_a of equation (7) might be used as an approximate[1] measure of the pitch angle, which is also given in Table 1. Unfortunately, ship motion measurements were not made on AP, so this pitch angle estimate cannot be validated. However, ship motion and orientation measurements are available from the ASP.

TABLE 1: AP main features in Poincaré sphere coordinates (ψ_c, χ_c).

Date	Wind speed	Wave height	DB	MID	Pitch
28 Mar.	7 kts	4 m	$(48.9°,-8.7°)$	$(50.9°,5.8°)$	$-2.7°$
30 Mar.	20 kts	5 to 6 m	$(36°,12.2°)$	$(45°,0.9°)$	$9.6°$

F.2 The Anne S Pierce (ASP)

ASP was imaged with orientations of $8°$ (line 1, referred to as L1P3) and $15°$ (line 6, pass 8 referred to as L6P8) from azimuth and at $39°$ and $35°$ incidence angles on March 28. As seen above, the mast near the middle and the two metallic features near the bow and the stern of the ship, referred to as MID, DF, and DB in Figure 2, are potential targets of symmetric scattering. Table 2 presents the coordinates (ψ_c, χ_c) on the Poincaré sphere of these features. They correspond to a signal to clutter ratio of about 20 dB, which results in a dispersion in phase of $\pm 5°$, according to the Rice distribution. The (MID) antenna ψ_c angle appears stable (within $3°$) during the 2 flights with an average scattering close to the dipole scattering angle. The two values of χ_c are about $30°$ apart. A deeper analysis of the ship responses reveals a focus error for the ship in L6P8; the ship trace is 50% longer for L6P8 as compared with L1P3. Focus errors can introduce a significant error in the peak intensity parameter, and the phase of the peak intensity is more sensitive to the focus setting than the intensity, as shown in [19], [27], [26]. This explains the large offset noted in χ_c, which directly relates to the trihedral-dihedral phase difference. In contrast, ψ_c, which depends strongly on the channel relative intensity, appears to be less affected by system focus errors. Consequently, unless the focus setting errors are removed, the information provided by the SSCM is not considered reliable.

The March 28 data, which appears to be better focused, can be used to estimate the ship orientation angles during data acquisition. Since the azimuth orientation angle is small ($15°$), the rotation angle ψ_a may be used as an approximate measure of the pitch angle. In fact, the MID rotation angle leads to a pitch angle measurement that is within $-0.2°$ of that measured on ASP, as shown in Table 2. The second

---

[1]The exact expression for the pitch angle measurement as a function of the rotation angle is given in [28].

data set, which suffers from the focus error, leads to an erroneous pitch estimate, as expected.

TABLE 2: ASP main features in Poincaré sphere coordinates (ψ_c, χ_c).

Line	Wind speed	Wave height	MID	DF	MID Pitch	DF Pitch	Meas.
L1P3	7 kts	4 m	(53.6°,2.3°)	(49.7°,24.5°)	-0.9°	-1.1°	-0.72
L6P8	7 kts	4 m	(50.7°,-30.3°)	(25.4°,-7.3°)	-9.4°	-16.3°	0.23°

.

V. CONCLUSIONS

Ship detection and characterization is a very complex problem, which is difficult to solve with conventional SARs that use a single polarization for transmission and a single polarization for reception. Fully polarimetric SARs, which provide unique information for target backscattering characterization, appear to be promising for ship detection and characterization. For calm sea surface conditions, the polarization anisotropy ΔS_n [21] offers a significant increase in ship-sea contrast at operational satellite SAR incidence angles (20° to 60°). For rougher sea surface conditions, the increasing heterogeneity of the ocean scattering mechanisms reduces the efficiency of the polarization anisotropy, which provides a slightly better ship-sea contrast than HV polarization. At near grazing incidence angles (larger than 55°), the polarization anisotropy is no longer effective, and HH polarization, which reduces the ocean return, remains the best candidate for ship detection.

The high resolution SSCM method introduced in [22] appears to be promising for ship characterization. The ability to identify elemental targets with a significant maximized symmetric scattering component, provides a ship specific distribution of "permanent" polarization scattering targets, which might be useful for ship identification under various wind and wave conditions. Such targets were used here to estimate the ASP pitch angle, for particular wind and wave conditions. In contrast to the polarization anisotropy discussed above, the SSCM seems to be less affected by rougher sea surface conditions; the mast on the AP demonstrated the same scattering type for both calm and rougher sea surface conditions. However, the SSCM, which strongly depends on the signal phase and the intensity of the peak signal, is sensitive to the system focus setting [19], [27] and Doppler centroid shifts [26]. These errors should be corrected prior to application of the SSCM method [28].

Further investigations are currently being conducted to confirm these results with other data sets. These encouraging results for ship detection and characterization should motivate the use of fully polarimetric satellite SAR data. The Upcoming launches of RADARSAT-2 and ALOS will make polarimetric data more accessible. However, this potential can only be exploited if the RADARSAT-2 and ALOS polarimetric modes are well calibrated.

REFERENCES

[1] D. Bicout and C. Brosseau. Multiply scattered waves through a spatially random medium: Entropy production and depolarization. *J. Phys. I France*, 2:2047–2063, 1992.

[2] W.L. Cameron, N. Youssef, and L.K. Leung. Simulated polarimetric signatures of primitive geometrical shapes. *IEEE Trans. Geoscience Rem. Sens.*, 34(3):793–803, 1996.

[3] R. Cloude and E. Pottier. A review of target decomposition theorems in radar polarimetry. *IEEE Trans. Geoscience Rem. Sens.*, 34(2):498–518, 1996.

[4] K. Eldhuset. An automatic ship and ship wake detection system for spaceborne SAR images in coastal regions. *IEEE Trans. Geoscience Rem. Sens.*, 34(4):1010–1019, 1996.

[5] R.H. Hawkins. Determination of antenna elevation pattern for airborne SAR using the rough target approach. *IEEE Trans. Geoscience Rem. Sens.*, 28(5):896–905, 1990.

[6] R.K. Hawkins, C.E. Brown, K.P. Murnaghan, J.R. Gibson, A. Alexander, and R. Marois. The SAR 580 facility-system update . In *Proc. 2002 Int. Geosc. Remote Sensing Symp., IGARSS'02* , Toronto, Canada, 2002.

[7] R.K. Hawkins, K.P. Murnaghan, M. Yeremy, and M. Rey. Ship detection using airborne polarimetric SAR. In *CEOS SAR Workshop Proc., Tokyo*, pages 6–15, April 2001.

[8] R.K. Hawkins, R. Touzi, A. Wind, K. Murnaghan, and C.E. Livingstone. Polarimetric calibration results and error budget for SAR-580 systems. In *Proc. of the CEOS SAR workshop, ESA SP-450, http://www.estec.esa.nl/CONFANNOUN/99b02*, October 1999.

[9] R.K. Hawkins, P. Vachon, J. Cranton, and K. Murnaghan. Scene descriptions for CV-580 SAR acquisitions St Margaret's Bay area. In *Report CCRS-TN-1998-021*, 1998.

[10] R.K. Hawkins, W. Wong, and K. Murnaghan. Crusade Experiment March 2000. In *Canada Centre for Remote Sensing CCRS-TN-2000-07*, March, 2000.

[11] J.R. Huynen. Measurement of the target scattering matrix . *Proc. IEEE*, 53(8):936–946, 1965.

[12] N. Ito, T. Hamazaki, and K. Tomioka. ALOS/PALSAR chracteristics and status. In *CEOS SAR Workshop Proc., Tokyo*, pages 191–194, April 2001.

[13] E. Krogager. New decomposition of the radar target scattering matrix. *Electronic Letters*, 26(18):1525–1527, 1990.

[14] C. E. Livingstone, A. L. Gray, R. K. Hawkins, P. W. Vachon, T. I. Lukowski, and M. LaLonde. The CCRS airborne SAR systems: Radar for remote sensing research. *Can. J. Rem. Sens.*, 21(4):468–491, 1995.

[15] A.P. Luscombe, K. Chotoo, and B.D. Huxtable. Polarimetric calibration of RADARSAT 2 . In *Proc. 2000 Int. Geosc. Remote Sensing Symp., IGARSS'00* , Honululu, Hawaii, 2000.

[16] H. Rais and A. W. Mansfield. L-Band/P-Band SAR Comparison for Search and Rescue: Recent Results . In *Proc. of the SPIE Aerosense Conference*, 5-9 April 1999, Orlando, Florida.

[17] M. T. Rey, J. K. E. Tunaley, and T. Sibald. Use of the Dempster-Shafer algorithm for the detection of SAR ship wakes. *IEEE Trans. Geoscience Rem. Sens.*, 31(5):1114–1118, 1993.

[18] R. Ringrose and N. Harris. Ship detection using polarimetric SAR data. In *Proc. of the CEOS SAR workshop, ESA SP-450, http://www.estec.esa.nl/CONFANNOUN/99b02*, October 1999.

[19] R. Touzi. Extraction of point target response characteristics from complex SAR data. *IEEE Trans. Geoscience Rem. Sens.*, 30:1158–1161, 1992.

[20] R. Touzi. Calibration and analysis of Convair-580 polarimetric SAR data for forest target characterization. Technical report, Final Report provided to the Defense Research Establishment of Ottawa (DREO) under the CCRS/DREO agreement FY97/98-98/99, June 1999.

[21] R. Touzi. Calibrated polarimetric SAR data for ship detection . In *Proc. 2000 Int. Geosc. Remote Sensing Symp., IGARSS'00* , Honululu, Hawaii, 2000.

[22] R. Touzi and F. Charbonneau. Characterization of target symmetric scattering using polarimetric SARs. *IEEE Trans. Geoscience Rem. Sens.*, 40, Nov., 2002.

[23] R. Touzi, S. Goze, T. Le Toan, A. Lopes, and E. Mougin. Polarimetric discriminators for SAR images. *IEEE Trans. Geoscience Rem. Sens.*, 30(5):973–980, 1992.

[24] R. Touzi, C. E. Livingstone, J. R. C. Lafontaine, and T. I. Lukowski. Consideration of antenna gain and phase patterns for calibration of polarimetric SAR data. *IEEE Trans. Geoscience Rem. Sens.*, 31(6):1132–1145, 1993.

[25] R. Touzi and C.E. Livingstone. A general method for the calibration of the C-band Convair-580 polarimetric SAR . In *Proc. of ASAR/CEOS 2003* , Montreal, Canada, 24-27 June 2003.

[26] R. Touzi and K. Raney. Effect of Doppler centroid mis-tracking on the Parameter estimation of point target complex signals. In *Proc. 1994 Int. Geosc. Remote Sensing Symp., IGARSS'94* , Pasadena, California, 1994.

[27] R. Touzi, K. Raney, and A. Lopes. On the use of complex SAR data for calibration. In *Proc. 1992 Int. Geosc. Remote Sensing Symp., IGARSS'92* , Houston, Texas, 1992.

[28] R. Touzi, R.K. Raney, and F. Charbonneau. On the use of symmetric scatterers for ship characterization. *IEEE Trans. Geoscience Rem. Sens.*, Submitted for publication, Sep. 2003.

[29] P. W. Vachon, J. W. M. Campbell, C. Bjerkelund, F. W. Dobson, and M. T. Rey. Ship detection by the RADARSAT SAR: Validation of detection model predictions. *Can. J. Rem. Sens.*, 23(1):48–59, March 1997.

[30] M. Yeremy, J.W.M. Campbell, K.Mattar, and T. Potter. Ocean surveillance with polarimetric SAR. *Can. J. Rem. Sens.*, 27(4):328–344, 2001.

[31] M. Zink, C. Buck, J.L. Suchail, R. Torres, A. Bellini, J. Closa, Y.L. Desnos, and B. Rosich. The radar imaging instrument and its applications: ASAR. In *ESA Bulletin, No. 106*, pages 46–55, June 2001.
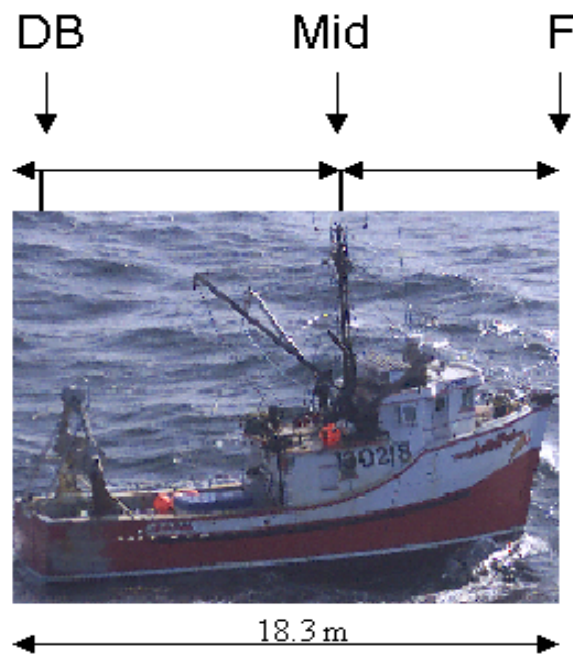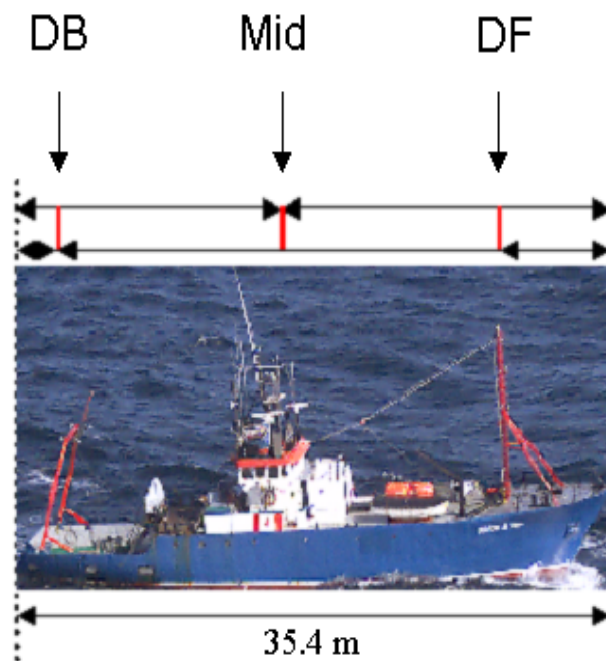
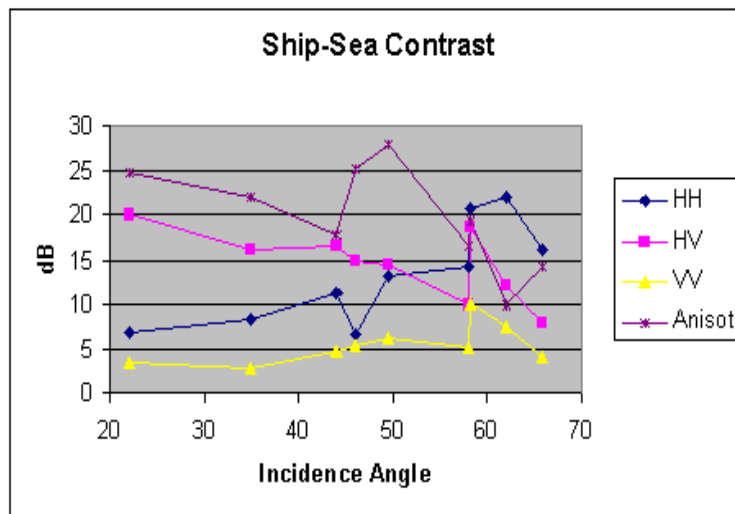Fig. 1. *Arctic Pride (AP)*

Fig. 2. *Anne S Pierce (ASP)*

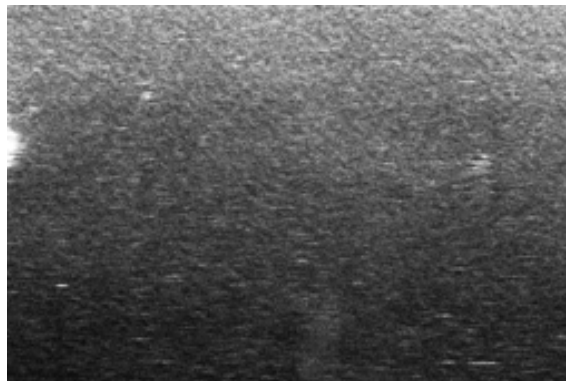Fig. 3. *Ship-sea contrast as a function of the incidence angle*

Fig. 4. *HH image. The top of the image is at 46° and the bottom is at 70° incidence angle*
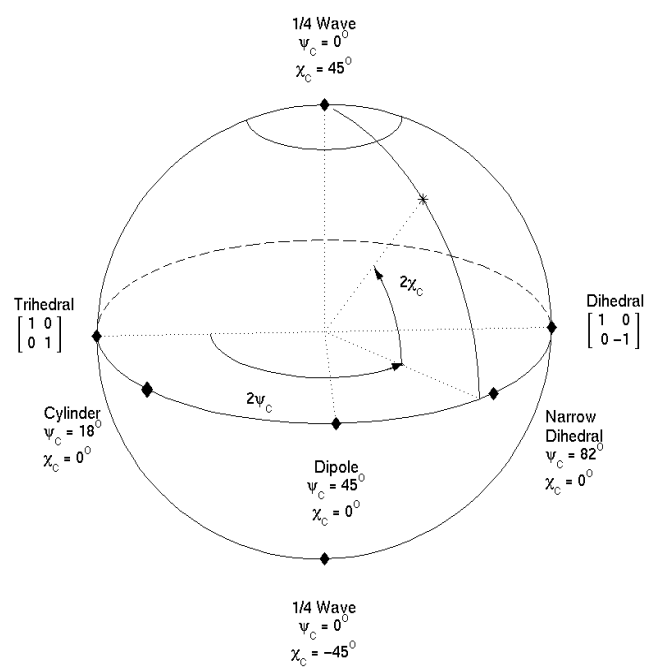

Fig. 5. *Polarization ansiotropy image*

Fig. 6. S_{sym}^{max} Target Sphere